High-Density Organic Electro-Optic Crystals for Ultra-Broadband THz Spectroscopy

Jin-Hong Seok, Uros Puc, Seung-Jun Kim, Woojin Yoon, Hoseop Yun, In Cheol Yu, Fabian Rotermund, Dongwook Kim, Mojca Jazbinsek,* and O-Pil Kwon*

Ultra-broadband THz photonics covering the 0.3–20 THz range provides a very attractive foundation for a wide range of basic research and industrial applications. However, the lack of ultra-broadband THz devices has yet to be overcome. In this work, high-density organic electro-optic crystals are newly developed for efficient THz wave generation in a very broad THz spectral range and are successfully used for a broadband THz time-domain spectroscopy. The new organic THz generator crystals, namely the OHP-TFS crystals, have very low void volume, high density, and are shown to cover the ultra-broadband THz spectrum up to about 15 THz, which cannot be easily accessed with the more widely used inorganic-based THz generators. In addition to the very favorable broadband properties, the generated THz electric-field amplitude at the pump wavelength of 1560 nm is about 40 times higher than that generated by a commercial inorganic THz generator (ZnTe crystal). By using the newly developed OHP-TFS as generation crystal in a compact table-top all-organic THz time-domain spectrometer based on a low-cost telecom fiber laser, the optical characteristics of a model material are successfully determined in the broad 1.5–12.5 THz range with high accuracy.

1. Introduction

The properties of THz waves differ significantly from those of higher frequency optical waves and lower frequency radio waves in the electromagnetic spectrum. Therefore, THz photonics opens new possibilities for both fundamental and industrial applications previously inaccessible in the optical and radio waves.[1–6] Ultra-broadband THz waves, which reside within the wide frequency range of 0.3–20 THz, have many advantages.

Specific optical phonons (and molecular vibrations) in materials have remarkably different THz excitation frequencies.[6–12] Consequently, many material parameters such as the refractive index, absorption coefficient, and conductivity vary at different THz frequencies in the wide range. However, the lack of ultra-broadband THz devices and materials, including generators and detectors blocks the proliferation of THz applications. Consequently, a lot of research effort has been devoted to enhancing the bandwidth of various types of THz generators and detectors.[13–15]

The realization of ultra-broadband THz devices with widely used inorganic materials is rather difficult. For example, zinc telluride (ZnTe), the most widely used inorganic semiconducting crystal, can generate high-energy and high-intensity THz waves that reach THz pulse energies of about 14 µJ and THz electric fields of about 570 kV cm^{-1}.[16–19] However, the corresponding THz bandwidth generated by inorganic crystals covers only the lower frequencies in the THz region (e.g., <3 THz for ZnTe). This is primarily because of the strong transverse phonon mode in the frequency range or the poor phase-matching between the optical pump and the generated THz waves.[13,15,20,21] A broader spectral bandwidth can be achieved using a very thin inorganic crystal (<0.1 mm) because of the reduced THz self-absorption and relaxed phase-matching restriction. However, because the optical-to-THz conversion

J. H. Seok, S. J. Kim, Prof. O. P. Kwon
Department of Molecular Science and Technology
Ajou University
Suwon 443-749, Korea
E-mail: opilkwon@ajou.ac.kr

The ORCID identification number(s) for the author(s) of this article can be found under https://doi.org/10.1002/adom.202100618.

Dr. U. Puc, Dr. M. Jazbinsek
Institute of Computational Physics
Zurich University of Applied Sciences (ZHAW)
Winterthur 8401, Switzerland
E-mail: mojca.jazbinsek@zhaw.ch

W. Yoon, Prof. H. Yun
Department of Chemistry & Department of Energy Systems Research
Ajou University
Suwon 443-749, Korea

I. C. Yu, Prof. F. Rotermund
Department of Physics
Korea Advanced Institute of Science and Technology (KAIST)
Daejeon 34141, Korea

Prof. D. Kim
Department of Chemistry
Kyonggi University
San 94–6, Iui-dong, Yeongtong-gu, Suwonsi, Gyeonggi 443-760, Korea

efficiency is proportional to the square of the thickness (at phase matching), the generated THz amplitude is relatively very small (e.g., one or two orders of magnitude smaller than those of the commonly used millimeter-thick crystals). Another benchmark inorganic crystal, nonlinear optical lithium niobate (LiNbO$_3$), that requires a complicated tilted pulse front excitation setup, shows a similar bandwidth limitation for THz generation. Photoconductive antennas utilizing inorganic semiconductors also mostly exhibit a relatively small bandwidth limited to few THz only. As for generation, the detection of THz waves using inorganic materials also shows the relatively small bandwidth due to the absorption and phase-matching limitations.

In addition to the inability to fulfill the ultra-broadband requirement in THz devices, many THz generators require bulky and expensive high-power laser systems, such as optical parametric amplifiers and regenerative amplifiers. Therefore, efficient THz generation materials that could be used even in more compact ultra-broadband THz spectroscopy systems covering the THz range beyond 10 THz are strongly desired. The introduction of organic materials is one potential route to overcome the bandwidth limitation of inorganic materials in THz systems.

In this work, we provide a design strategy for organic electro-optic crystals having high-density for efficient ultra-broadband THz wave generation. The newly designed organic crystals consist of yellow-color, linear rod-shaped cationic chromophores and non-color anions that possess both tight packing and multiple interionic interaction abilities. The crystals therefore have very small void volume and high density. The results show ultra-broadband and efficient THz generation at frequencies of up to about 15 THz. The amplitude of the THz electric field generated by the organic crystals is about 40 times higher than that generated by their inorganic counterpart (ZnTe crystal). The table-top all-organic THz time-domain spectroscopy system based on a newly developed organic THz generator thereby allows the characterization of optical properties (the refractive index and the absorption coefficient) of a model sample to be measured over a broad THz range with a high accuracy.
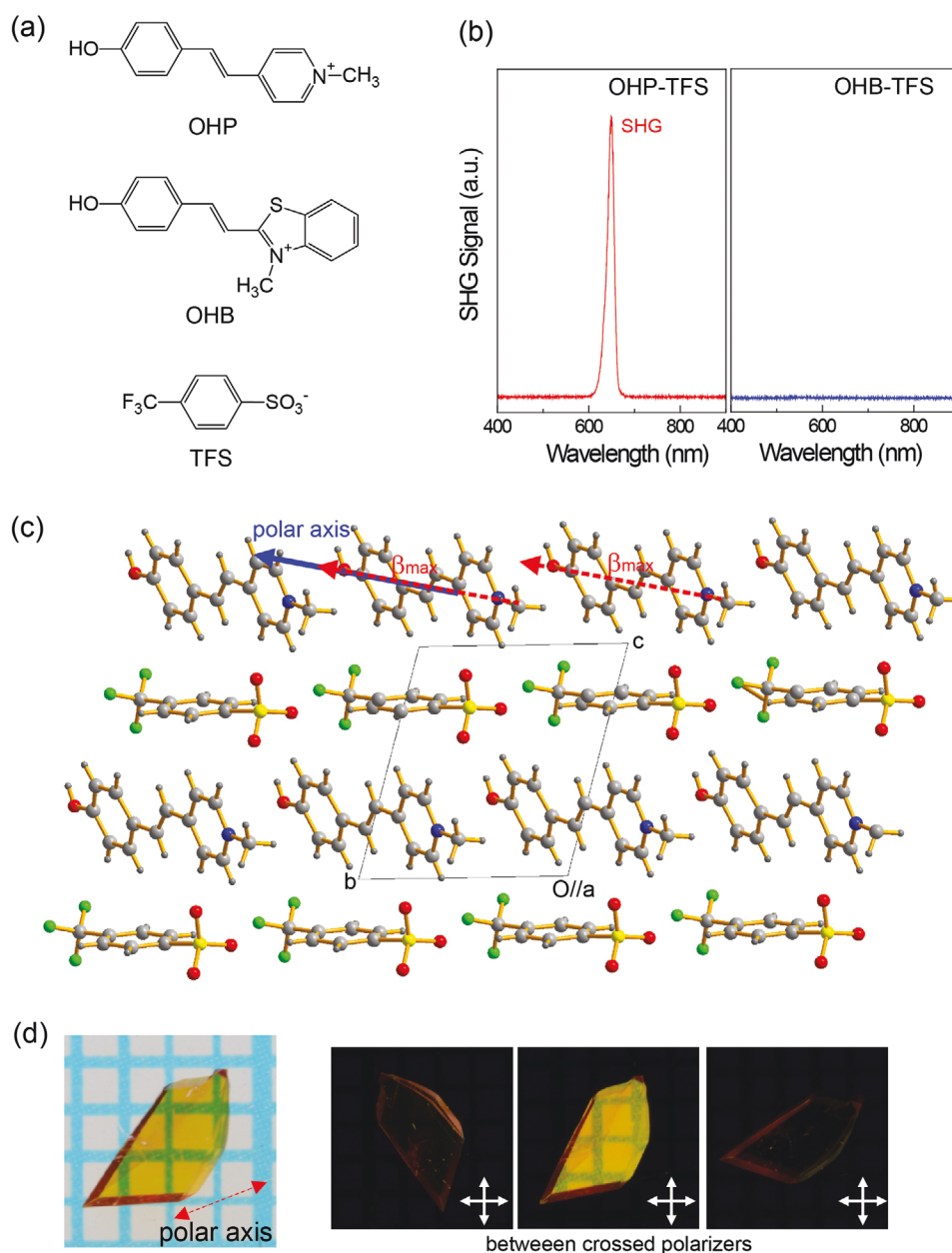
2. Results and Discussions

2.1. Design of High-Density Organic Electro-Optic Crystals

Figure 1a shows the chemical structure of the newly designed high-density nonlinear optical crystals. To achieve ultra-broadband THz wave generation with simple collinear setups, the nonlinear optical crystals should possess the following properties: i) large macroscopic second-order optical nonlinearity, ii) good phase matching (velocity matching) between the optical and THz waves, and iii) small optical and THz wave absorption.[21–26] We consider these three requirements in the design of the new nonlinear optical crystals in this work. To obtain a large macroscopic nonlinear optical coefficient in the crystal (effective hyperpolarizability tensor components $\beta_{ijk}^{\mathrm{eff}}$ of ≥100 × 10^{-30} esu), strong electron-withdrawing pyridinium and benzothiazolium are introduced to the OHP (4-(4-hydroxystyryl)-1-methylpyridinium-1-ium) and

OHB (2-(4-hydroxystyryl)-3-methylbenzothiazol-3-ium) cations, respectively. Moreover, to achieve good phase matching between the infrared wavelength of the optical pump beam and the generated THz waves, yellow-color cationic chromophores are introduced. In previous studies, yellow-color cations with an absorption maximum wavelength $\lambda_{\max}$ near 400 nm exhibited a high probability of achieving good phase-matching at the optical pump wavelengths of 1140–1300 nm and above.[22,23] When a strong electron-donating dialkylamino group is introduced with strong electron-withdrawing pyridinium or benzothiazolium groups in chromophores, the absorption maximum wavelength $\lambda_{\max}$ shifts to near 500 nm.[26–28] Therefore, in this work, we selected the phenolic electron donor group as it has a relatively weak electron donating strength. The counter anion, a noncolor 4-(trifluoromethyl)benzenesulfonate (TFS) anion was used for both crystals.

To achieve ultra-broadband THz generation, it is important that the organic electro-optic crystals have a small amplitude of vibrational modes.[21] The vibrational motions, including the phonon modes in organic electro-optic crystals (i.e., THz generator), lead to self-absorption of the generated THz waves.[10] For inorganic electro-optic crystals such as ZnTe, GaP, and LiNbO$_3$, the phonon-induced self-absorption is relatively large, which typically limits the generation and detection bandwidth of these materials up to few THz only. Note that the damage threshold of organic electro-optic crystals may be lower than for inorganic crystals at the same experimental conditions. However, the damage threshold of organic electro-optic crystals is not a problem for relatively low-fluence optical pump pulses such as used in this work as well as the pump wavelength well above the absorption range of these crystals. In addition, introducing yellow-color cations (OHP and OHB) in this work is an asset considering possible photostability issues compared to other benchmark organic crystals (red or orange color) because of the lower wavelength of absorption maximum (i.e., further away from the optical pump wavelength and also from the two-photon absorption wavelength). Therefore, we consider organic electro-optic crystals as very suitable for ultra-broadband THz spectroscopy systems, especially in simple collinear set-ups based on low-power, relatively low-cost, and compact femtosecond lasers. However, the vibrational modes still limit the achievable dynamic range with organic crystals at certain THz frequencies.[10,29]

To reduce the vibrational amplitude in the crystal, a decrease of the void volume (and increase in density) and an increase in the interionic interactions in the design are required. A large void volume may result in a large vibrational amplitude. Here, all the cations and anions can be packed tightly and have multiple interionic interaction ability. The OHP and OHB cations possess a simple flat rod shape that can be compactly stacked together with small steric hindrance. In addition, all the cations and anions consist of almost fully π-conjugated systems (i.e., without non-π-conjugated aliphatic groups). The π-conjugated structure can induce various types of interionic attractive interactions due to partially negative-charged π-electron and partially positive-charged hydrogen substituents.[30] The phenolic —OH substituents on the cations and the —SO$_3^-$ and —CF$_3$ substituents on the anions possess multiple hydrogen-bonding abilities.[31–34]

ADVANCED
SCIENCE NEWS

www.advancedsciencenews.com

ADVANCED
OPTICAL
MATERIALS

www.advopticalmat.de

Figure 1. a) Chemical structure of the newly designed organic crystals OHP-TFS and OHB-TFS. b) Qualitative powder SHG measurements of OHP-TFS and OHB-TFS at the fundamental wavelength of 1300 nm: spectrum of the reflected signal. c) Perfectly parallel alignment of nonlinear optical cations in OHP-TFS crystals: the solid and the dotted arrows respectively represent the direction of the polar axis and the main microscopic charge transfer axis projected to the plane normal to the crystallographic a-axis. d) Photographs of an as-grown OHP-TFS crystal with the direction of the polar axis determined using a polarizer.

2.2. Large Optical Nonlinearity with Good Phase Matching Possibility

To investigate whether the newly designed organic crystals OHP-TFS and OHB-TFS exhibit non-centrosymmetric or centrosymmetric arrangements of their respective nonlinear optical cations OHP and OHB, qualitative powder second harmonic generation (SHG) measurements[35,36] were performed at the fundamental wavelength of 1300 nm. As shown in Figure 1b, OHP-TFS showed a strong SHG signal, while

no SHG signal was observed for OHB-TFS. This shows that OHP-TFS crystals exhibit a noncentrosymmetric crystal structure and therefore, second-order nonlinearity, while OHB-TFS crystals exhibit a centrosymmetric structure. To investigate the molecular ordering of OHP-TFS crystals in more detail, single-crystal X-ray structure analysis was performed. OHP-TFS crystals exhibit a noncentrosymmetric P1 crystal structure. The details are listed in the Supporting Information. As shown in Figure 1c, in OHP-TFS crystals, the nonlinear optical OHP cations show a perfectly parallel alignment, which results in

the maximum value of the diagonal effective hyperpolarizability tensor element β_{111}^{eff}. The OHP-TFS crystals have a very large diagonal component of the effective hyperpolarizability tensor β_{111}^{eff} (125×10^{-30} esu). The value of the diagonal component was evaluated based on the microscopic first hyperpolarizability β_{max} of OHP cations (125×10^{-30} esu) obtained from density functional theory (DFT) calculations and the perfectly parallel packing of the OHP cations.[37,38]

The diagonal nonlinear optical coefficient of OHP-TFS crystals (125×10^{-30} esu) is a comparable to the values in benchmark organic THz crystals; for example, nonionic OH1 (2-(3-(4-hydroxystyryl)-5,5-dimethylcyclohex-2-enylidene) malononitrile) crystals (63×10^{-30} esu) and ionic OHQ-T (2-(4-hydroxystyryl)-1-methylquinolinium 4-methylbenzenesulfonate) crystals (121×10^{-30} esu), DAST (4-(4-(N,N-dimethylamino)styryl)-1-methylpyridinium 4-methylbenzenesulfonate) crystals (161×10^{-30} esu), and DSTMS ((4-(4-(N,N-dimethylamino)styryl)-1-methylpyridinium 2,4,6-trimethylbenzenesulfonate) crystals (151×10^{-30} esu).[27,38–42] As shown in Figure S1, Supporting Information, the absorption maximum wavelength λ_{max} of OHP-TFS in methanol is 392 nm. Therefore, OHP-TFS crystals satisfy two of the requirements:

they have large macroscopic optical nonlinearity ($\beta_{111}^{eff} \geq 100 \times 10^{-30}$ esu), and are based on yellow chromophores, which may allow for good phase matching across a large range of infrared wavelengths. In addition, OHP-TFS crystals exhibit a relatively low absorption in the THz range as discussed in Section 2.4.

2.3. High Density with Very Low Void Volume

As mentioned above, the vibrational amplitude in the crystal is related to the void volume and the interionic interaction strength, which are, to some extent, correlated. **Figure 2** shows representative strong interionic interactions in OHP-TFS crystals that were analyzed using Hirshfeld surface analysis.[43–45] The flat rod-shaped OHP cations possess a planar conformation and are tightly packed with one another through cation–cation interactions in a cation layer (Figure 2a). In an anion layer, the TFS anions form multiple strong hydrogen bonds (anion–anion interactions, Figure 2b). With many cation–anion interactions (Figure 2c), OHP-TFS crystals exhibit 3D network-like interionic interactions between the cation layers and anion
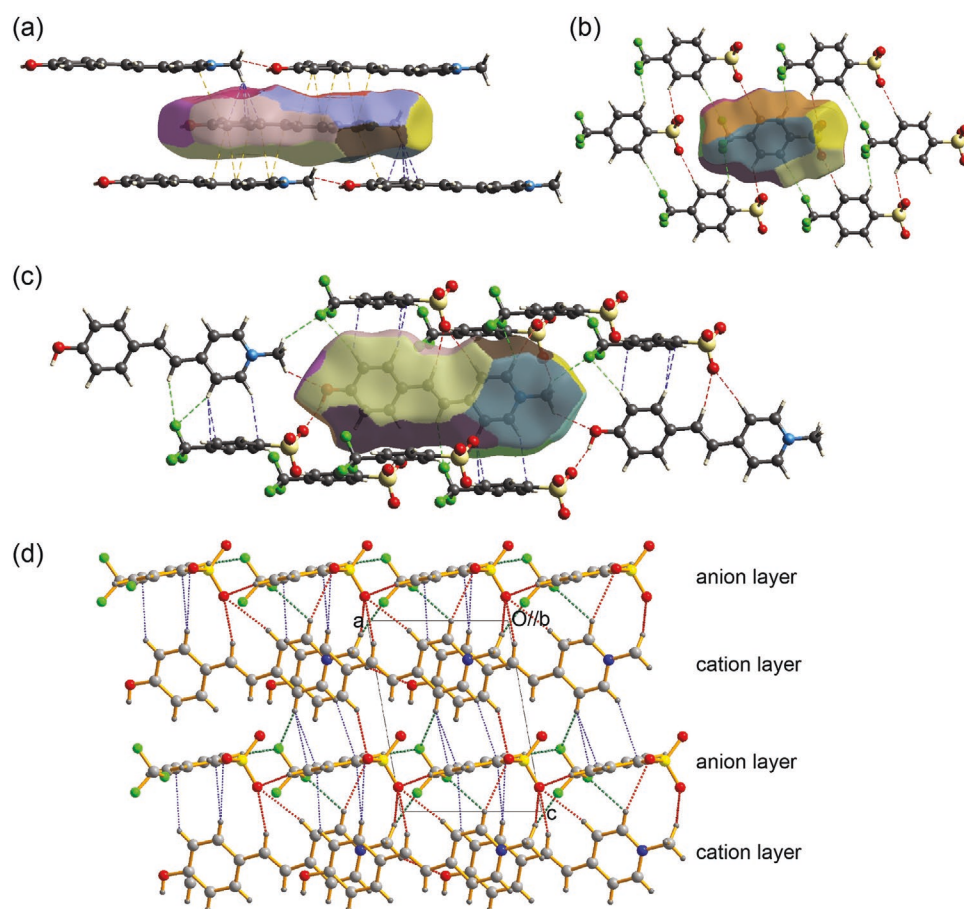
Figure 2. Representative strong interionic interactions. Hirshfeld surface analysis with fragment patch of a,c) OHP cation and b) TFS anion in OHP-4TFS crystals: a) cation–cation interactions in a cation layer (O···H, (Ar)C···H, and π–π stacking C···C (Ar···Ar or Ar···C = C), b) anion–anion interactions in an anion layer (O···H, F···H), c) cation–anion interactions (O···H, F···H, and (Ar)C···H). d) 3D network-like interionic interactions between cation layers and anion layers (O···H, F···H, and (Ar)C···H). The red, green, blue, and yellow dotted lines present X···Y close contacts of O···H (≤ 2.80 Å), F···H (≤ 2.80 Å), (Ar)C···H (≤ 3.06 Å), and π–π stacking C···C (≤ 3.60 Å), respectively.

layers (Figure 2d). These strong and multiple interionic interactions may reduce the vibrational amplitude and, additionally, the void volume in the crystal.

In Table S1, Supporting Information, the density and void volume[46] in the unit cell of OHP-TFS crystals are listed. For comparison, those of various state-of-the-art organic nonlinear optical crystals are also listed. Among these crystals, OHP-TFS crystals exhibit the lowest void volume content and the highest density. Therefore, the molecular (and phonon) vibrations may be strongly suppressed in OHP-TFS crystals.

In addition, the macroscopic nonlinear optical susceptibility $\chi_{111}^{(2)}$, which is relevant for all frequency conversion applications, is proportional to the chromophore number density N and the effective hyperpolarizability tensor element β_{111}^{eff} ($\chi_{111}^{(2)} \propto N\beta_{111}^{eff}$).[39] Therefore, the high density of chromophores is also beneficial for the macroscopic nonlinear optical susceptibility, which is an additional advantage of the newly developed OHP-TFS crystals.

2.4. Ultra-Broadband Efficient THz Wave Generation

The newly developed OHP-TFS crystals exhibit a perfectly parallel orientation and high-density packing of the nonlinear optical cations, resulting in a large macroscopic second-order optical nonlinearity. They also show a relatively low wavelength of maximal absorption (yellow color) and are therefore expected to have good phase matching for nonlinear optical frequency conversion from the infrared to the THz frequency range. To investigate THz wave generation characteristics of OHP-TFS

crystals, we prepared bulk single crystals and used them as THz generation crystals in a table-top THz system.[29]

Figure 1d shows photographs of an as-grown OHP-TFS crystal that shows good optical quality and suitable morphology for optical experiments. The largest crystal facet of the OHP-TFS crystals used in this work is the (001) plane; therefore, the polar axis of OHP-TFS is practically parallel to the main crystal facet (Figure S3, Supporting Information), which is optimal for THz wave generation by optical rectification in a simple collinear geometry. The optical pump and probe beams in our setup (**Figure 3**a) are from a 38 fs, 1560 nm compact fiber-based laser with a 100 MHz repetition rate and 190 mW average output power (Menlo Systems). The OHP-TFS crystal was aligned normal to the propagation direction with the polar axis parallel to the polarization of the pump beam. For coherent electro-optic detection, we used the so-called THz-induced lensing principle[47] in the same configuration as described previously.[29] Note that we use THz-induced lensing because the standard electro-optic sampling (EOS) with inorganic ZnTe and GaP is of limited use in our case due to the strongly limited detection efficiency and bandwidth of these crystals at the 1560 nm wavelength of the probe beam. In addition, organic electro-optic crystals cannot be used with the standard EOS detection principle owing to their high birefringence. In this work, for THz-induced lensing detector we employed organic DSTMS (4-(4-(N,N-dimethylamino)styryl)-1-methylpyridinium 2,4,6-trimethylbenzenesulfonate[27] from Rainbow Photonics AG) crystal, which has well-known optical and THz material parameters for detection.[29,48] All THz experiments in this work
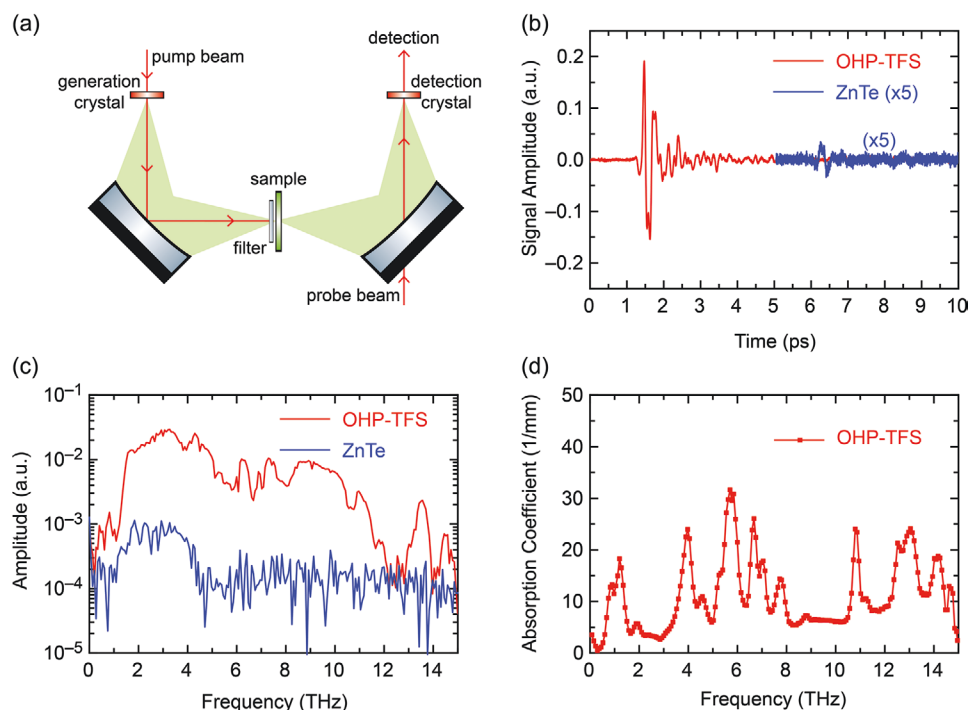
Figure 3. THz wave generation in OHP-TFS: a) THz generation/detection and spectroscopy set-up with the 1560 nm pump and probe beams. b) Time- and c) frequency-domain amplitudes of the THz waves generated in a 0.31 mm thick OHP-TFS and in a 1.0 mm thick ZnTe crystal. Note that for ZnTe, the amplitude is magnified by a factor of five in (b). d) Absorption coefficient of OHP-TFS in the THz frequency region.

**ADVANCED
SCIENCE NEWS**
www.advancedsciencenews.com

**ADVANCED
OPTICAL
MATERIALS**
www.advopticalmat.de

were performed at room temperature in dry air environment with the relative humidity below 5%.

For comparison, we also tested a standard 1.0 mm-thick (110)-oriented ZnTe crystal as the generation crystal while keeping all the other experimental conditions identical. As shown in Figure 3b, the THz electric field (peak-to-peak amplitude) generated by a 0.31 mm-thick OHP-TFS crystal is approximately 40 times stronger than that generated by ZnTe. In addition, the spectrum of OHP-TFS is ultra-broadband and extends up to about 15 THz, while the bandwidth in ZnTe is limited to about 4 THz. This is because of the i) higher nonlinearity, ii) more optimal phase-matching at the 1560 nm pump wavelength, and iii) lower phonon-mode absorption of OHP-TFS compared to ZnTe in the THz frequency range.

The spectrum of the generated THz field by OHP-TFS is relatively flat across the very broadband range of 1.5–12 THz. It is particularly interesting that the THz generation efficiency of the OHP-TFS generator in the high-frequency THz range (≈9 THz) is not much lower than that in the lower-frequency range (≈3 THz). Note that the dimples in the obtained spectra (Figure 3c) originate from the molecular vibrations of both the THz generation and detection crystals (OHP-TFS and DSTMS, respectively).

Consequently, OHP-TFS crystals have shown to simultaneously achieve a high efficiency (40 times higher generated THz field than ZnTe at 1560 nm) and ultra-high bandwidth (up to about 15 THz) in THz wave generation. In many organic and inorganic nonlinear optical and semiconducting THz generators based on femtosecond pump lasers, although strong THz electric field can be achieved, the THz generation efficiency in the high-frequency THz range is considerably lower than that in low-frequency THz range.[13,14,39,49–51] For semiconductor antenna-based generators, which can be also used in combination with compact femtosecond sources at 1560 nm, the bandwidth is also typically limited to few THz only. Recently, metallic spintronic THz generators have also been shown to exhibit excellent THz generation performance; for example, both a strong THz electric field of 300 kV cm⁻¹ and gapless ultra-broadband range (covering to 20–30 THz) have been demonstrated.[52–54] Note that currently, the optical-to-THz conversion efficiency of metallic spintronic THz generators at 800 nm is comparable to millimeter-thick ZnTe crystals.[54]

The ultra-broadband spectrum of the OHP-TFS generator is related to absorption characteristics in the THz range. Figure 3d shows the absorption coefficient of OHP-TFS crystal measured in the same setup using another DSTMS crystal as the generator. The absorption coefficient in the THz range of OHP-TFS crystals is very favorable and the peaks are lower than in many other benchmark organic ionic and nonionic crystals. In the whole THz frequency range measured, OHP-TFS crystals exhibit much lower absorption peaks than ionic DAST and DSTMS crystals.[11,29] In particular, compared to other ionic benchmark DSTMS crystals, the absorption of OHP-TFS is considerably reduced in the higher-frequency THz range above 7 THz.[29,48] This is very important because compared to lower THz frequency ranges, satisfying the phase-matching condition in this frequency range is a much larger challenge due to the phase mismatch being, in general, proportional to the frequency of the wave generated by difference frequency generation or optical rectification.[15] Also the nonionic benchmark OH1 crystals show several strong absorption peaks with very large absorption coefficient of over 300 cm⁻¹.[55–57] The relative flatness and high amplitude of the generated THz spectrum, as shown in Figure 3b and 3c, is very promising for accurate THz spectroscopy, as demonstrated below.
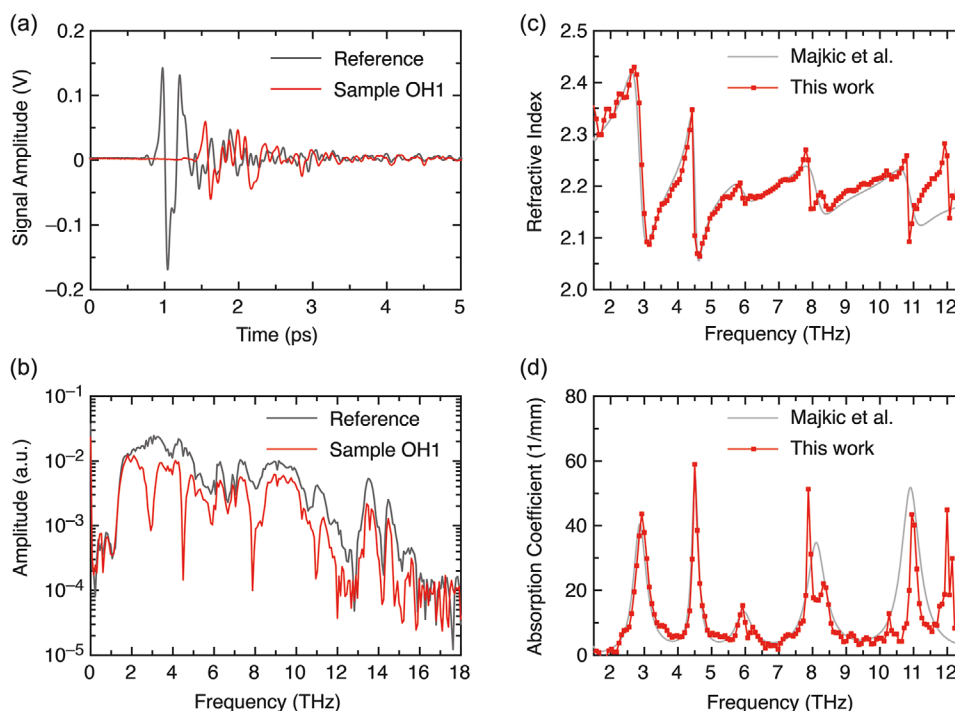
2.5. Ultra-Broadband THz Spectroscopy

To demonstrate the operation of the all-organic THz time-domain spectrometer with the newly developed OHP-TFS crystal as a THz generator, we performed a high-accuracy measurement of the refractive index and absorption of a model sample in the ultra-broadband range of 1.5–12.5 THz. We chose an OH1 (2-(3-(4-hydroxystyryl)-5,5-dimethylcyclohex-2-enylidene)malononitrile) nonlinear optical crystal as the sample. This material has many phonon modes within the frequency range.[55–57] The measured characteristics of the OH1 crystal along the polar axis in the THz frequency region are compared to the previous values measured by time-domain spectroscopy[56,57] and frequency-domain spectroscopy.[55]

The analysis of the refractive index and the absorption is based on comparing the reference signal (generated by OHP-TFS and detected with DSTSM) without the OH1 sample and the signal with the OH1 sample (see **Figure 4**a) using the same experimental setup (Figure 3a). For the analysis, we adopted the approximation of neglecting multiple reflections of the THz wave in the sample. Considering the amplitude difference (Figure 4b) and the phase difference $\Delta\varphi$ between both measurements, we evaluated the refractive index (Figure 4c) and the absorption coefficient (Figure 4d) of OH1 following the standard analysis.[58] The thickness of the OH1 sample, 0.145 mm, was determined by comparing the phase difference $\Delta\varphi$ to literature values.[56,57] Should there be a systematic error in the thickness in the previous reports, the value of the refractive index shown in Figure 4c would be vertically shifted, but the features would remain identical.

Compared to previous measurements, we observed some additional details, such as the double absorption peak at around 8 THz (see Figure 4d). These features agree with the theoretical calculations of the absorption modes in OH1 and the measurements based on the frequency-domain spectroscopy.[55] This result indicates that highly accurate and sensitive broadband time-domain spectroscopy is possible with the newly developed OHP-TFS crystal as the THz generator in a table-top THz system. We also note here that we have not noticed any stability issues with OHP-TFS crystals (any noticeable change of the optical appearance or the degradation of the THz generation performance) during the experiments reported in this work.

3. Conclusions

In summary, the newly developed, high-efficiency OHP-TFS nonlinear optical crystals, having high density, low void volume, and yellow color, exhibit efficient ultra-broadband THz wave generation at up to ≈15 THz, which overcomes the bandwidth limitation of widely used inorganic-based THz

**ADVANCED
SCIENCE NEWS**

www.advancedsciencenews.com

**ADVANCED
OPTICAL
MATERIALS**

www.advopticalmat.de

Figure 4. Demonstration of ultra-broadband THz spectroscopy based on OHP-TFS generator with a model sample (0.145 mm-thick OH1 crystal): a) Time-domain signals generated in OHP-TFS without (reference) and with the OH1 sample and b) the corresponding amplitude spectrum. c) The extracted refractive index and d) absorption coefficient are compared to the Lorentz fit of a previous measurement at up to about 11 THz by Majkic et al.[56]

generators. Additionally, the OHP-TFS crystals generated relatively very high THz electric field amplitudes that are about 40 times larger than the 1.0 mm-thick ZnTe inorganic benchmark crystals. The optical properties (refractive index and absorption coefficient) of the model OH1 crystal in the 1.5–12.5 THz range were successfully determined with high accuracy using a compact table-top THz time-domain spectrometer with OHP-TFS as the THz generation crystal. Therefore, developing high-density organic crystals with large nonlinearity is very attractive for ultra-broadband THz photonics.

4. Experimental Section

The details of the synthesis, UV–vis absorption characteristics, X-ray crystal structure analysis, crystal structures, and quantum chemical calculations are described in the Supporting Information.

Supporting Information

Supporting Information is available from the Wiley Online Library or from the author.

Conflict of Interest

The authors declare no conflict of interest.

Data Availability Statement

Research data are not shared.

[1] T. Kampfrath, K. Tanaka, K. A. Nelson, *Nat. Photonics* **2013**, *7*, 680.

[2] X. Chen, D. Hu, R. Mescall, G. You, D. N. Basov, Q. Dai, M. Liu, *Adv. Mater.* **2019**, *31*, 1804774.

[3] K. S. Kumar, G. L. Prajapati, R. Dagar, M. Vagadia, D. S. Rana, M. Tonouchi, *Adv. Opt. Mater.* **2019**, *8*, 1900958.

[4] H. A. Hafez, X. Chai, A. Ibrahim, S. Mondal, D. Férachou, X. Ropagnol, T. Ozaki, *J. Opt.* **2016**, *18*, 093004.

[5] W. Zouaghi, M. D. Thomson, K. Rabia, R. Hahn, V. Blank, H. G. Roskos, *Eur. J. Phys.* **2013**, *34*, S179.

[6] X. Yang, X. Zhao, K. Yang, Y. Liu, Y. Liu, W. Fu, Y. Luo, *Trends Biotechnol.* **2016**, *34*, 810.

[7] F. Perakis, L. De Marco, A. Shalit, F. Tang, Z. R. Kann, T. D. Kühne, R. Torre, M. Bonn, Y. Nagata, *Chem. Rev.* **2016**, *116*, 7590.

[8] J. B. Baxter, G. W. Guglietta, *Anal. Chem.* **2011**, *83*, 4342.

[9] K. L. Nguyen, T. Friščić, G. M. Day, L. F. Gladden, W. Jones, *Nat. Mater.* **2007**, *6*, 206.

[10] J. Kim, Y. C. Park, J. H. Seok, M. Jazbinsek, O. P. Kwon, *Adv. Opt. Mater.* **2021**, *9*, 2001521.

[11] P. D. Cunningham, L. M. Hayden, *Opt. Express* **2010**, *18*, 23620.

[12] A. G. Davies, A. D. Burnett, W. Fan, E. H. Linfield, J. E. Cunningham, *Mater. Today* **2008**, *11*, 18.

[13] J. A. Fülöp, S. Tzortzakis, T. Kampfrath, *Adv. Opt. Mater.* **2019**, *8*, 1900681.

[14] M. Tonouchi, *Nat. Photonics* **2007**, *1*, 97.

[15] L. R. Dalton, P. Gunter, M. Jazbinsek, O. P. Kwon, P. A. Sullivan, *Organic Electro-Optics and Photonics: Molecules, Polymers and Crystals*, Cambridge University Press, Cambridge **2015**, Ch. 10.

[16] G. Polónyi, B. Monoszlai, G. Gäumann, E. J. Rohwer, G. Andriukaitis, T. Balciunas, A. Pugzlys, A. Baltuska, T. Feurer, J. Hebling, J. A. Fülöp, *Opt. Express* **2016**, *24*, 23872.

[17] J. A. Fülöp, G. Polónyi, B. Monoszlai, G. Andriukaitis, T. Balciunas, A. Pugzlys, G. Arthur, A. Baltuska, J. Hebling, *Optica* **2016**, *3*, 1075.

[18] T. Löffler, T. Hahn, M. Thomson, F. Jacob, H. G. Roskos, *Opt. Express* **2005**, *13*, 5353.

[19] F. Blanchard, L. Razzari, H.-C. Bandulet, G. Sharma, R. Morandotti, J.-C. Kieffer, T. Ozaki, M. Reid, H. F. Tiedje, H. K. Haugen, F. A. Hegmann, *Opt. Express* **2007**, *15*, 13212.

[20] A. Leitenstorfer, S. Hunsche, J. Shah, M. C. Nuss, W. H. Knox, *Appl. Phys. Lett.* **1999**, *74*, 1516.

[21] J. Hebling, K. L. Yeh, M. C. Hoffmann, B. Bartal, K. A. Nelson, *J. Opt. Soc. Am. B* **2008**, *25*, B6.

[22] C. U. Jeong, B. J. Kang, S. H. Lee, S. C. Lee, W. T. Kim, M. Jazbinsek, W. Yoon, H. Yun, D. Kim, F. Rotermund, O. P. Kwon, *Adv. Funct. Mater.* **2018**, *28*, 1801143.

[23] M. H. Shin, W. T. Kim, S. I. Kim, S. J. Kim, I. C. Yu, S. W. Kim, M. Jazbinsek, W. Yoon, H. Yun, F. Rotermund, O. P. Kwon, *Adv. Sci.* **2020**, *7*, 2001738.

[24] G. A. Valdivia-Berroeta, E. W. Jackson, K. C. Kenney, A. X. Wayment, I. C. Tangen, C. B. Bahr, S. J. Smith, D. J. Michaelis, J. A. Johnson, *Adv. Funct. Mater.* **2020**, *30*, 1904786.

[25] J. Shi, H. He, F. Liang, X. Zhang, D. Xu, J. Yao, G. Zhang, Z. Hu, J. Yao, Y. Wu, *J. Mater. Chem. C* **2020**, *8*, 4226.

[26] S. Kannan, A. Sekar, K. Sivaperuman, *J. Mater. Chem. C* **2020**, *8*, 16668.

[27] Z. Yang, L. Mutter, M. Stillhart, B. Ruiz, S. Aravazhi, M. Jazbinsek, A. Schneider, V. Gramlich, P. Günter, *Adv. Funct. Mater.* **2007**, *17*, 2018.

[28] S. C. Lee, B. J. Kang, J. A. Lee, S. H. Lee, M. Jazbinšek, W. Yoon, H. Yun, F. Rotermund, O. P. Kwon, *Adv. Opt Mater.* **2018**, *6*, 1701258.

[29] U. Puc, T. Bach, P. Günter, M. Zgonik, M. Jazbinsek, *Adv. Photonics Res.* **2021**, *2*, 2000098.

[30] C. A. Hunter, K. R. Lawson, J. Perkins, C. J. Urch, *J. Chem. Soc., Perkin Trans. 2* **2001**, *5*, 651.

[31] M. H. Shin, S. H. Lee, B. J. Kang, M. Jazbinšek, W. Yoon, H. Yun, F. Rotermund, O. P. Kwon, *Adv. Funct. Mater.* **2018**, *28*, 1805257.

[32] S. H. Lee, B. J. Kang, B. W. Yoo, S. C. Lee, S. J. Lee, M. Jazbinsek, H. Yun, F. Rotermund, O. P. Kwon, *Adv. Funct. Mater.* **2017**, *27*, 1605583.

[33] D. Kim, W. T. Kim, J. H. Seok, I. C. Yu, M. Jazbinsek, W. Yoon, H. Yun, D. Kim, F. Rotermund, O. P. Kwon, *J. Mater. Chem. C* **2020**, *8*, 10078.

[34] S. J. Lee, B. J. Kang, M. H. Shin, S. C. Lee, S. H. Lee, M. Jazbinsek, H. Yun, D. Kim, F. Rotermund, O. P. Kwon, *Adv. Opt. Mater.* **2018**, *6*, 1700930.

[35] S. K. Kurtz, T. T. Perry, *J. Appl. Phys.* **1968**, *39*, 3798.

[36] I. Aramburu, J. Ortega, C. L. Folcia, J. Etxebarria, *Appl. Phys. Lett.* **2014**, *104*, 071107.

[37] S. J. Kwon, O. P. Kwon, J. I. Seo, M. Jazbinsek, L. Mutter, V. Gramlich, Y. S. Lee, H. Yun, P. Günter, *J. Phys. Chem. C* **2008**, *112*, 7846.

[38] P. J. Kim, J. H. Jeong, M. Jazbinsek, S. J. Kwon, H. Yun, J. T. Kim, Y. S. Lee, I. H. Baek, F. Rotermund, P. Günter, O. P. Kwon, *CrystEngComm* **2010**, *13*, 444.

[39] S. H. Lee, M. Jazbinsek, C. P. Hauri, O. P. Kwon, *CrystEngComm* **2016**, *18*, 7180.

[40] O. P. Kwon, S. J. Kwon, M. Jazbinsek, F. D. J. Brunner, J. I. Seo, C.h. Hunziker, A. Schneider, H. Yun, Y. S. Lee, P. Günter, *Adv. Funct. Mater.* **2008**, *18*, 3242.

[41] S. H. Lee, B. J. Kang, J. S. Kim, B. W. Yoo, J. H. Jeong, K. H. Lee, M. Jazbinsek, J. W. Kim, H. Yun, J. Kim, Y. S. Lee, F. Rotermund, O. P. Kwon, *Adv. Opt. Mater.* **2015**, *3*, 756.

[42] S. R. Marder, J. W. Perry, W. P. Schaefer, *Science* **1989**, *245*, 626.

[43] M. A. Spackman, J. J. McKinnon, *CrystEngComm* **2002**, *4*, 378.

[44] M. A. Spackman, D. Jayatilaka, *CrystEngComm* **2009**, *11*, 19.

[45] J. J. McKinnon, D. Jayatilaka, M. A. Spackman, *Chem. Commun.* **2007**, *37*, 3814.

[46] Mercury 4.3.0 program (2020.0 release), Cambridge Crystallographic Data Centre (CCDC), https://www.ccdc.cam.ac.uk (accessed: 2020).

[47] A. Schneider, I. Biaggio, P. Günter, *Appl. Phys. Lett.* **2004**, *84*, 2229.

[48] M. Stillhart, A. Schneider, P. Günter, *J. Opt. Soc. Am. B* **2008**, *25*, 1914.

[49] E. Castro-Camus, M. Alfaro, *Photon. Res.* **2016**, *4*, A36.

[50] K. Reimann, *Rep. Prog. Phys.* **2007**, *70*, 1597.

[51] M. Savoini, L. Huber, H. Cuppen, E. Abreu, M. Kubli, M. J. Neugebauer, Y. Duan, P. Beaud, J. Xu, T. Rasing, S. L. Johnson, *ACS Photonics* **2018**, *5*, 671.

[52] T. Seifert, S. Jaiswal, U. Martens, J. Hannegan, L. Braun, P. Maldonado, F. Freimuth, A. Kronenberg, J. Henrizi, I. Radu, E. Beaurepaire, Y. Mokrousov, P. M. Oppeneer, M. Jourdan, G. Jakob, D. Turchinovich, L. M. Hayden, M. Wolf, M. Münzenberg, M. Kläui, T. Kampfrath, *Nat. Photonics* **2016**, *10*, 483.

[53] T. Seifert, S. Jaiswal, M. Sajadi, G. Jakob, S. Winnerl, M. Wolf, M. Kläui, T. Kampfrath, *Appl. Phys. Lett.* **2017**, *110*, 252402.

[54] Z. Feng, H. Qiu, D. Wang, C. Zhang, S. Sun, B. Jin, W. Tan, *J. Appl. Phys.* **2021**, *129*, 010901.

[55] J. Kim, S. H. Lee, S. C. Lee, M. Jazbinsek, K. Miyamoto, T. Omatsu, Y. S. Lee, O. P. Kwon, *J. Phys. Chem. C* **2016**, *120*, 24360.

[56] A. Majkić, M. Zgonik, A. Petelin, M. Jazbinšek, B. Ruiz, C. Medrano, P. Günter, *Appl. Phys. Lett.* **2014**, *105*, 141115.

[57] F. D. J. Brunner, O. P. Kwon, S. J. Kwon, M. Jazbinsek, A. Schneider, P. Günter, *Opt. Express* **2008**, *16*, 16496.

[58] P. U. Jepsen, *J. Infrared, Millimeter, Tetrahertz Waves* **2019**, *40*, 395.

2100618 (8 of 8)